Published in final edited form as:
Radiat Prot Dosimetry. 2006 ; 122(1-4): 521–527. doi:10.1093/rpd/ncl448.

CHALLENGES AND PROGRESS IN PREDICTING BIOLOGICAL RESPONSES TO INCORPORATED RADIOACTIVITY

R.W. Howell[1], **P.V.S.V. Neti**[1], **M. Pinto**[1], **B.I. Gerashchenko**[1], **V.R. Narra**[2], and **E.I. Azzam**[1]

[1]Department of Radiology, UMDNJ – New Jersey Medical School, Newark, NJ 07103, USA

[2]Department of Radiation Oncology, The Cancer Institute of New Jersey, UMDNJ–Robert Wood Johnson Medical School, New Brunswick, NJ 08854, USA

Abstract

Prediction of risks and therapeutic outcome in nuclear medicine largely rely on calculation of the absorbed dose. Absorbed dose specification is complex due to the wide variety of radiations emitted, nonuniform activity distribution, biokinetics, etc. Conventional organ absorbed dose estimates assumed that radioactivity is distributed uniformly throughout the organ. However, there have been dramatic improvements in dosimetry models that reflect the substructure of organs as well as tissue elements within them. These models rely on improved nuclear medicine imaging capabilities that facilitate determination of activity within voxels that represent tissue elements of about 0.2 – 1 cm^3. However, even these improved approaches assume that all cells within the tissue element receive the same dose. The tissue element may be comprised of a variety of cells having different radiosensitivities and different incorporated radioactivity. Furthermore, the extent to which nonuniform distributions of radioactivity within a small tissue element impact the absorbed dose distribution is strongly dependent on the number, type, and energy of the radiations emitted by the radionuclide. It is also necessary to know whether the dose to a given cell arises from radioactive decays within itself (self-dose) or decays in surrounding cells (cross-dose). Cellular response to self-dose can be considerably different than its response to cross-dose from the same radiopharmaceutical. Bystander effects can also play a role in the response. Evidence shows that even under conditions of "uniform" distribution of radioactivity, a combination of organ dosimetry, voxel dosimetry and dosimetry at the cellular and multicellular levels can be required to predict response.

INTRODUCTION

Prediction of radiation risks and therapeutic outcome in nuclear medicine largely relies on calculation of the absorbed dose. However, accurate specification of absorbed dose is hampered by many factors, among them heterogeneous tissue composition, nonuniform distribution of radioactivity in organs and tissues, and complex clearance kinetics. Following administration of a radiopharmaceutical, radioactivity is taken up by various organs within the body and is then eliminated through both biological clearance and physical decay. To provide a consistent and organized approach to estimate absorbed doses from tissue incorporated radioactivity, a general formalism was developed by the Medical Internal Radiation Dose (MIRD) Committee of the Society of Nuclear Medicine (1–3).

The MIRD formalism has traditionally been used to calculate mean organ absorbed doses for the purpose of risk estimation in diagnostic nuclear medicine. This approach was driven, in part, by medical imaging technologies that enabled determination of organ activity. Mean organ absorbed dose estimates assume that radioactivity is distributed uniformly throughout the organ (4). Major improvements in nuclear medicine imaging technology have facilitated determination of activity within tissue elements that are represented by voxels with volumes of about 0.2 cm^3. This capability made it possible to obtain absorbed dose distributions with

spatial detail commensurate with voxel size (5). As a consequence, there have been dramatic improvements in MIRD dosimetry models that reflect the substructure of organs as well as tissue elements within them (6–8). Further advances in these techniques continue (9–12).

Although improvements in nuclear medicine imaging technology have enabled us to specify absorbed dose at increasingly small spatial scales, limitations on spatial resolution require one to assume that all cells within the tissue element receive essentially the same absorbed dose. However, any given tissue element that is represented by a voxel may be comprised of a variety of cells having very different amounts of incorporated radioactivity (13–15). Furthermore, the tissue element may be composed of an assortment of cells having very different radiosensitivities (16). Accordingly, the absorbed dose delivered to the various cells in the tissue element may differ markedly as well as their biological response (17–21). To address some of these issues, the MIRD Committee published a monograph that provided a first step toward simplifying calculation of absorbed dose to the cell from intracellularly localized radioactivity (22).

It is clear that a combination of organ dosimetry, voxel dosimetry and dosimetry at the cellular and multicellular levels will be required to accurately predict biological response to nonuniform distributions of radioactivity. The microdosimetry community has long recognized the importance of the microscopic distribution of radioactivity on absorbed dose specification and ultimately biological response (23). Yet, experimentally validated approaches that can predict biological responses to nonuniform distributions of radioactivity are generally not available at the cellular level. This article describes the challenges and progress in understanding the biological effects caused by tissue-incorporated radioactivity and the development of multicellular dosimetry approaches to predict the response. Finally, the potential for fusing organ, voxel and multicellular dosimetry techniques to predict biological responses *in vivo* are discussed.

CHARACTERISITICS OF RADIONUCLIDES

Emitted radiations

The extent to which nonuniform distributions of radioactivity within a small tissue element impact the absorbed dose distribution, and ultimately the biological effect, is strongly dependent on the number, type, and energy of the radiations emitted by the radionuclide. Many radionuclides used in nuclear medicine decay by electron capture and/or internal conversion (e.g. ^{67}Ga, ^{99m}Tc, ^{111}In, ^{123}I, ^{125}I, ^{201}Tl) and consequently emit a large number of low-energy Auger electrons. The majority of these electrons deposit their energy over subcellular dimensions and therefore produce nonuniform dose distributions (24,25). Similarly, the short range of alpha particles in biological tissues (40–100 μm) also leads to nonuniform dose distributions from ^{222}Rn and other alpha particle emitters of potential use in nuclear medicine (25–28). Energetic beta emitters such as ^{90}Y have a greater degree of cross-irradiation because their mean range in tissue is at least several hundred μm. However, the nonuniform distribution of these radionuclides invariably leads to nonuniform dose distributions as well (5,21,29,30). Finally, the beta particles emitted by ^{3}H deposit their energy over short distances.

Relative biological effectiveness

While it is essential to consider the dose distributions that arise from nonuniform distributions of radioactivity, it is also necessary to know whether the dose to a given cell arises from radioactive decays within itself (self-dose) or decays in surrounding cells or other parts of the body (cross-dose). Cellular response to self-dose delivered by a radiopharmaceutical can be considerably different than its response to cross-dose from the same radiopharmaceutical. This is well known for Auger emitters where the RBE of the self-dose can be an order of magnitude

greater than the cross-dose (31). We have observed this for beta emitters as well where the self-dose from ^{131}I was 3 times more lethal than the cross-dose (see below) (32).

NONUNIFORM DISTRIBUTION OF RADIOACTIVITY IN TISSUE ELEMENTS

Multicellular Cluster Model

A simple three dimensional tissue model was developed to study biological effects of nonuniform distributions of radioactivity at the multicellular level. As described in detail elsewhere (33–35), this was accomplished by assembling 7.9 mg (~ 0.0079 cm^3) multicellular clusters containing 4×10^6 V79 Chinese hamster cells wherein 1%, 10%, 50%, or 100% of the cells were radiolabeled and randomly located in the cluster. Thus, from a voxel perspective the activity distribution might be considered uniform, however, at the multicellular level, the distribution is clearly nonuniform. The multicellular clusters were then maintained at 10.5°C for 72 h after which they were dispersed and the cells seeded for colony formation. Thus, with this model, the variables affecting distribution of radioactivity can be tightly controlled.

Nonuniform distributions of ^{131}I

The 3D multicellular cluster model was used to examine the impact of nonuniformities at the multicellular level on the lethal effects of ^{131}I (35). When 100% of the cells were labeled with ^{131}I-iododeoxyuridine (^{131}IdU), the surviving fraction of cells in the cluster was exponentially dependent on the cluster activity down to 0.1% survival. The lack of a shoulder in the response to this low-LET β-particle emitter is likely due to its incorporation into the DNA (32,35,36). When 10% of the cells were labeled, it was observed that the survival fraction began to saturate at about 1% survival. Absorbed dose estimates revealed that the mean lethal cluster doses were 4.5, 5.7, and 6.4 Gy for 100%, 10%, and 1% labeling, respectively. Based on these data, it was concluded that when the distribution of ^{131}I is uniform at the macroscopic level, but nonuniform at the multicellular level, the mean absorbed dose to a tissue element may not be a suitable quantity for use in predicting biological effect of ^{131}I.

Subsequent studies were carried with this model to determine the effects of ^{131}IdU individually on the labeled and unlabeled cells (32). In these studies the labeled cells were dyed with CFDA-SE and the labeled (dyed) and unlabeled (undyed) cells were separately seeded for colony formation using a fluorescence activated cell sorter (FACS). Unlabeled cells received only a cross-dose. In contrast, the labeled cells received both a self-dose and cross-dose. Isolating the effects of the self-dose showed that it was about 3.3 times more radiotoxic per unit dose than the cross-dose. Thus, the self-dose delivered by ^{131}IdU has a higher RBE than the cross-dose. It appears that the higher RBE for the self-dose is related to the location in which the ^{131}I decays occur in these cells (e.g. within the DNA) (32,35,36). With this in mind, it is worth noting that similar RBE values have also been reported for cell killing by DNA-incorporated ^{3}H (emits very low energy β particles) compared to tritiated water (37).

Nonuniform distributions of ^{210}Po

Multicellular cluster survival data have also been obtained when cells were labeled with ^{210}Po-citrate. About 72% of this radiochemical localizes in the cytoplasm and 28% in the nucleus (38). Figure 1 shows the surviving fraction of cells in the multicellular cluster as a function of the cluster dose when 1%, 10%, 100% of the cells were radiolabeled. Calculation of the mean absorbed dose to the cluster yielded D_{37} values of 1.1, 0.76, and 0.70 Gy for 1%, 10%, 100% labeling with ^{210}Po-citrate, respectively. In contrast, the D_{37} value for chronic ^{137}Cs γ-rays was 12 Gy (33–35). All three ^{210}Po survival curves, including the 100% labeling curve, exhibited saturation despite the alpha particles range of > 5 cell diameters and the fact that each cell has about 12 neighbors. As noted above, ^{131}IdU exhibited a similar

saturation, whereas, irradiation with chronic external ^{137}Cs γ-rays produced a classic shouldered survival curve without saturation that is characteristic of low-LET radiations (35).

Modeling response with multicellular dosimetry

It is apparent that even under these "ideal" conditions, the mean absorbed dose to a very small tissue element may not be a suitable quantity for use in predicting biological effects of alpha particle emitters (e.g. ^{210}Po) and relatively long-range beta emitters (e.g. ^{131}I). Initial modeling of the killing of labeled and unlabeled cells was achieved by considering the cellular self- and cross-doses and the fraction of cells labeled (39).

$$SF = f\, e^{-D_{self}/D_{37,self}} e^{-D_{cross}/D_{37,cross}} + (1-f) e^{-D_{cross}/D_{37,cross},}$$

where D_{self} is the mean self-dose to the labeled cell, D_{cross} is the mean cross dose received by the labeled and unlabeled cells, f is the fraction of cells labeled, and $D_{37,self}$ and $D_{37,cross}$ are the mean lethal self- and cross-doses, respectively. This approach was used to model the observed responses for ^{210}Po-citrate (not shown) and ^{131}IdU (39). The model afforded an excellent fit to the first two logs of killing in all three labeling cases (1%, 10%, 100%). This shows the promise of using multicellular dosimetry models to predict response. However, this model was not successful at predicting the response beyond the second log of killing due to the saturation in the experimental survival curves.

Nonuniform uptake of radioactivity by labeled cells

In the cases of ^{210}Po and ^{131}I, survival curves for 10% labeling exhibited saturation despite the high degree of cross-irradiation afforded under these conditions by both ^{131}I and ^{210}Po (Fig. 1). The survival curve for 100% labeling with ^{210}Po also saturated to some degree (Fig. 1). These are important findings in that they have significant consequences for therapeutic use and risk estimation for these and similar radionuclides. We hypothesize that this saturation is related to a combination of variations in uptake of radioactivity by labeled cells and the geometry or shape of the cluster. Geometry can have a significant impact on dose distribution. Even when all cells in a spherical cluster contain the same ^{131}I activity, cells at the center of a spherical cluster receive double the cross-dose received by those at the periphery. Measurements of our multicellular clusters show that the geometry of the cluster is a paraboloid capped with a cylindrical wedge. This geometry, coupled with nonuniformities in uptake of radioactivity (see below), can lead to an even wider range of cellular doses. Autoradiographic studies which quantify the *relative* cellular uptake of ^{210}Po-citrate have revealed a log normal distribution of radioactivity per labeled cell (40). This broad log normal distribution has emerged even though all of the cells in a uniform suspension were exposed to the same extracellular concentration of ^{210}Po-citrate. A similar distribution was observed for ^{131}IdU. Initial modeling calculations show that this activity distribution can result in survival curves that saturate in a manner analogous to those observed in Fig. 1 (40). More detailed Monte Carlo modeling is under way with the ultimate goal of matching the observed survival curves.

BYSTANDER EFFECTS

Recent developments in radiobiology have shown that irradiated cells can prompt biological responses in neighboring unirradiated cells. These phenomena are known as bystander effects. Numerous studies on bystander effects have been observed following external beam irradiation of a variety of cell types in a number of cell culture models, as well as *in vivo* models (41). Observed bystander effects include genetic alterations (mutations, micronucleus formation), neoplastic transformation, changes in gene expression and cellular redox status, induction of apoptosis, alteration of proliferation, and modulation of cell cycle check points (42).

Furthermore, genomic instability is thought to be mediated via bystander mechanisms (43). Bystander effects have been shown to be mediated by gap-junction intercellular (GJIC) communication (41,44,45) and by signaling via diffusible secreted factors (46,47). Bystander effects can be modulated by oxidative metabolism (41,48,49). These findings and their implications have been extensively discussed in a number of review articles that address the bystander effect (50,51).

Bystander effects from nonuniform distributions of radioactivity

These findings suggest that bystander effects are highly relevant to the biological effects of nonuniform distributions of radioactivity. This is borne out by our experimental data in three dimensional cell cultures held at 10.5°C that demonstrates bystander cell killing in unlabeled cells adjacent to cells labeled with ^{3}HTdR or ^{125}IdU (33,34,52). Using a similar model, Persaud et al. have observed bystander cell killing when 20% of the cells were labeled with ^{3}HTdR (53). In addition, they showed that the ^{3}HTdR labeled cells imparted mutagenic effects on their neighbors. Xue et al. used an *in vivo* tumor model to show that labeling cells with ^{125}IdU led to an antiproliferative response in the bystander cells (54). Surprisingly, when cells were labeled with ^{123}IdU, an Auger electron emitter with similar properties to ^{125}I, a proliferative bystander response was observed (A.I. Kassis, data presented at this meeting – Microdosimetry 2005).

Proliferative bystander responses have also been observed in monolayer cultures of unlabeled cells adjacent to cells labeled with ^{3}HTdR (55). This response was shown to depend on the percentage of cells labeled, with ≥50% being required (56). In this model, the proliferative bystander response did not appear to be mediated by either gap junctional intercellular communication or long range factors released from the irradiated cells (57).

Additional bystander studies have been carried out in our laboratory with three dimensional cultures of apparently normal human fibroblasts growing in Cytomatrix™ carbon scaffolds. In these studies, cells were co-pulse-labeled *in situ* with ^{3}H-deoxycytidine and bromodeoxyuridine (BrdU). Using this labeling approach, only cells in S-phase were labeled (3–16% of total population) and the labeled cells were identified using standard anti-BrdU flow cytometric approaches. Induction of a G1 checkpoint in bystander cells was assayed by monitoring the transition from G1 to S phase using uptake of iododeoxyuridine (IdU) and a three-parameter flow cytometry technique. It was determined that dose rates to the labeled cells up to 0.32 Gy/h did not induce any significant G1 checkpoint in the unlabeled bystander cells. It is possible that no significant stress-induced effects were observed because the dose rates were insufficient and/or the percentage of cells labeled was not high enough to elicit a bystander response. Details of these studies are presented in a companion manuscript in this issue of Radiation Protection Dosimetry (Pinto et al.).

It is clear that a variety of bystander responses can be elicited by radiolabeled cells. The type and magnitude of the response depend on the radionuclide, percentage of cells labeled, self-absorbed dose to the cells, and tissue microenvironment. It is clear that modeling the biological response of cells to nonuniform distributions of radioactivity solely on the basis of absorbed dose may not adequately predict response even when the dose is calculated at the cellular level. This is of importance to risk estimation in diagnostic nuclear medicine and radiation protection (radon, radiological terrorism), as well as clinical outcome in therapeutic nuclear medicine.

CONCLUSIONS

Prediction of biological responses to incorporated radioactivity will require a comprehensive dosimetry approach. Ultimately, knowledge of absorbed dose at the cellular level is essential. The dose to any given cell is delivered by radiations emitted by radioactivity in the given cell

(self-dose) as well as radioactivity in other locations in the body (cross-dose). Cross-doses are delivered by decays in organs afar and in nearby tissue elements (voxels). These cross-doses can be obtained with the aid of modern nuclear medicine imaging techniques. Additional cross-dose arises from decays in neighboring cells within the same tissue element. Multicellular approaches such as those described herein are required for this contribution. The cellular self-dose can be calculated using standard cellular S value approaches. Careful bookkeeping is required to keep track of the self- and cross-doses from each type of radiation so that their respective RBE values can be applied. Finally, multicellular dose response modeling will be required to account for these variables as well as those relating to bystander effects.

REFERENCES

1. Loevinger, R.; Berman, M. A revised schema for calculating the absorbed dose from biologically distributed radionuclides. New York: Society of Nuclear Medicine; 1976.
2. Loevinger, R.; Budinger, TF.; Watson, EE. MIRD Primer for Absorbed Dose Calculations. New York: The Society of Nuclear Medicine; 1991.
3. ICRU. Methods of Assessment of Absorbed Dose in Clinical use of Radionuclides, Report 32. Bethesda, MD: International Commission on Radiation Units and Measurements; 1979.
4. Snyder, WS.; Ford, MR.; Warner, GG.; Watson, SB. "S," absorbed dose per unit cumulated activity for selected radionuclides and organs. New York: Society of Nuclear Medicine; 1975.
5. Sgouros G, Chiu S, Pentlow KS, Brewster LJ, Kalaigian H, Baldwin B, Daghighian F, Graham MC, Larson SM, Mohan R. Three-dimensional dosimetry for radiotherapy treatment planning. J. Nucl. Med 1993;34:1595–1601. [PubMed: 8394886]
6. Bouchet LG, Bolch WE, Weber DA, Atkins HL, Poston JW. MIRD Pamphlet No. 15: Radionuclide S values in a revised model of the adult head and brain. J. Nucl. Med 1999;40:62S–101S. [PubMed: 10086719]
7. Bolch WE, Bouchet LG, Robertson JS, Wessels BW, Siegel JA, Howell RW, Erdi AK, Aydogan B, Costes S, Watson EE. MIRD Pamphlet No. 17: The dosimetry of nonuniform activity distributions - radionuclide S values at the voxel level. J. Nucl. Med 1999;40:11S–36S. [PubMed: 9935083]
8. Bouchet LG, Bolch WE, Blanco HP, Wessels BW, Siegel JA, Rajon DA, Clairand I, Sgouros G. MIRD Pamphlet No 19: absorbed fractions and radionuclide S values for six age-dependent multiregion models of the kidney. J Nucl Med 2003;44:1113–1147. [PubMed: 12843230]
9. Guy MJ, Flux GD, Papavasileiou P, Flower MA, Ott RJ. RMDP: a dedicated package for ^{131}I SPECT quantification, registration and patient-specific dosimetry. Cancer Biother Radiopharm 2003;18:61–69. [PubMed: 12667309]
10. Ljungberg M, Frey E, Sjogreen K, Liu X, Dewaraja Y, Strand SE. 3D absorbed dose calculations based on SPECT: evaluation for 111-In/90-Y therapy using Monte Carlo simulations. Cancer Biother Radiopharm 2003;18:99–107. [PubMed: 12667313]
11. McKay E. A software tool for specifying voxel models for dosimetry estimation. Cancer Biother Radiopharm 2003;18:379–392. [PubMed: 12954124]
12. Sgouros G, Kolbert KS, Sheikh A, Pentlow KS, Mun EF, Barth A, Robbins RJ, Larson SM. Patient-specific dosimetry for ^{131}I thyroid cancer therapy using ^{124}I PET and 3-dimensional-internal dosimetry (3D-ID) software. J Nucl Med 2004;45:1366–1372. [PubMed: 15299063]
13. Jönsson B-A, Strand S-E, Larsson BS. A quantitative autoradiographic study of the heterogeneous activity distribution of different indium-111-labeled radiopharmaceuticals in rat tissues. J. Nucl. Med 1992;33:1825–1832. [PubMed: 1403151]
14. Makrigiorgos GM, Adelstein SJ, Kassis AI. Cellular radiation dosimetry and its implications for estimation of radiation risks. Illustrative results with technetium-99m-labeled microspheres and macroaggregates. JAMA 1990;264:592–595. [PubMed: 2366298]
15. Makrigiorgos GM, Ito S, Baranowska-Kortylewicz J, Vinter DW, Iqbal A, Van den Abbeele AD, Adelstein SJ, Kassis AI. Inhomogeneous deposition of radiopharmaceuticals at the cellular level: Experimental evidence and dosimetric implications. J. Nucl. Med 1990;31:1358–1363. [PubMed: 2384804]

16. Oakberg EF. Spermatogonial stem-cell renewal in the mouse. Anat. Rec 1971;169:515–532. [PubMed: 5550531]

17. Feinendegen, LE.; Bond, VP.; Booz, J. ICRU NEWS. Bethesda, MD: International Commission on Radiation Units and Measurements; 1994. The quantification of physical events within tissue at low levels of exposure to ionizing radiation; p. 9-12.

18. NCRP. Tritium and other radionuclide labelled organic compounds incorporated in genetic material, Report No. 63. National Council on Radiation Protection and Measurements. 1979

19. Wessels BW, Griffith MH. Miniature thermoluminescent dosimeter absorbed dose measurements in tumor phantom models. J. Nucl. Med 1986;27:1308–1314. [PubMed: 3734904]

20. Humm JL, Cobb LM. Nonuniformity of tumor dose in radioimmunotherapy. J. Nucl. Med 1990;31:75–83. [PubMed: 2295944]

21. Humm JL, Macklis RM, Bump K, Cobb LM, Chin LM. Internal dosimetry using data derived from autoradiographs. J. Nucl. Med 1993;34:1811–1817. [PubMed: 8410302]

22. Goddu, SM.; Howell, RW.; Bouchet, LG.; Bolch, WE.; Rao, DV. MIRD Cellular S values: self-absorbed dose per unit cumulated activity for selected radionuclides and monoenergetic electron and alpha particle emitters incorporated into different cell compartments. Reston, VA: Society of Nuclear Medicine; 1997.

23. Fisher DR, Harty R. The microdosimetry of lymphocytes irradiated by alpha-particles. Int. J. Radiat. Biol 1982;41:315–324.

24. Makrigiorgos GM, Adelstein SJ, Kassis AI. Limitations of conventional internal dosimetry at the cellular level. J. Nucl. Med 1989;30:1856–1864. [PubMed: 2809750]

25. Goddu SM, Rao DV, Howell RW. Multicellular dosimetry for micrometastases: dependence of self-dose versus cross-dose to cell nuclei on type and energy of radiation and subcellular distribution of radionuclides. J. Nucl. Med 1994;35:521–530. [PubMed: 8113908]

26. Humm JL, Chin LM. A model of cell inactivation by alpha-particle internal emitters. Radiat. Res 1993;134:143–150. [PubMed: 8488249]

27. Roeske JC, Stinchcomb TG. Dosimetric framework for therapeutic alpha-particle emitters. J. Nucl. Med 1997;38:1923–1928. [PubMed: 9430471]

28. Akabani G, Kennel SJ, Zalutsky MR. Microdosimetric analysis of alpha-particle-emitting targeted radiotherapeutics using histological images. J Nucl Med 2003;44:792–805. [PubMed: 12732682]

29. Kwok CS, Prestwich WV, Wilson BC. Calculation of radiation doses for nonuniformly distributed beta and gamma radionuclides in soft tissue. Med. Phys 1985;12:405–412. [PubMed: 4033585]

30. Erdi AK, Wessels BW, DeJager R. Tumor activity confirmation and isodose curve display for patients receiving iodine-131-labelled 16.88 human monoclonal antibody. Cancer 1994;73:932–944. [PubMed: 8306282]

31. Humm JL, Howell RW, Rao DV. Dosimetry of Auger electron emitting radionuclides: Report No.3 of the AAPM Nuclear Medicine Task Group No. 6. Med. Phys 1994;21:1901–1915. [PubMed: 7700197]

32. Neti PVSV, Howell RW. Isolating effects of microscopic nonuniform distributions of ^{131}I on labeled and unlabeled cells. J. Nucl. Med 2004;45:1050–1058. [PubMed: 15181140]

33. Bishayee A, Hill HZ, Stein D, Rao DV, Howell RW. Free-radical initiated and gap junction-mediated bystander effect due to nonuniform distribution of incorporated radioactivity in a three-dimensional tissue culture model. Radiat. Res 2001;155:335–344. [PubMed: 11175669]

34. Bishayee A, Rao DV, Howell RW. Evidence for pronounced bystander effects caused by nonuniform distributions of radioactivity using a novel three-dimensional tissue culture model. Radiat. Res 1999;152:88–97. [PubMed: 10428683]

35. Neti PVSV, Howell RW. When may a nonuniform distribution of ^{131}I be considered uniform? An experimental basis for multicellular dosimetry. J. Nucl. Med 2003;44:2019–2026. [PubMed: 14660728]

36. Bishayee A, Rao DV, Bouchet LG, Bolch WE, Howell RW. Radioprotection by DMSO against cell death caused by intracellularly localized I-125, I-131, and Po-210. Radiat. Res 2000;153:416–427. [PubMed: 10761002]

37. Straume T, Carsten AL. Tritium radiobiology and relative biological effectiveness. Health Phys 1993;65:657–672. [PubMed: 8244712]

38. Howell RW, Rao DV, Hou D-Y, Narra VR, Sastry KSR. The question of relative biological effectiveness and quality factor for Auger emitters incorporated into proliferating mammalian cells. Radiat. Res 1991;128:282–292. [PubMed: 1961925]
39. Howell RW, Neti PV. Modeling multicellular response to nonuniform distributions of radioactivity: differences in cellular response to self-dose and cross-dose. Radiat Res 2005;163:216–221. [PubMed: 15658898]
40. Neti PVSV, Howell RW. Log normally distributed cellular uptake of radioactivity: Implications for biological responses to radiopharmaceuticals. J Nucl Med under revision. 2006
41. Azzam EI, de Toledo SM, Little JB. Oxidative metabolism, gap junctions and the ionizing radiation-induced bystander effect. Oncogene 2003;22:7050–7057. [PubMed: 14557810]
42. Goldberg Z, Lehnert BE. Radiation-induced effects in unirradiated cells: a review and implications in cancer. Int J Oncol 2002;21:337–349. [PubMed: 12118330]
43. Clutton SM, Townsend KM, Walker C, Ansell JD, Wright EG. Radiation-induced genomic instability and persisting oxidative stress in primary bone marrow cultures. Carcinogenesis 1996;17:1633–1639. [PubMed: 8761419]
44. Azzam EI, de Toledo SM, Gooding T, Little JB. Intercellular communication is involved in the bystander regulation of gene expression in human cells exposed to very low fluences of alpha particles. Radiat Res 1998;150:497–504. [PubMed: 9806590]
45. Azzam EI, de Toledo SM, Little JB. Expression of CONNEXIN43 is highly sensitive to ionizing radiation and other environmental stresses. Cancer Res 2003;63:7128–7135. [PubMed: 14612506]
46. Mothersill C, Seymour CB. Cell-cell contact during gamma irradiation is not required to induce a bystander effect in normal human keratinocytes: evidence for release during irradiation of a signal controlling survival into the medium. Radiat Res 1998;149:256–262. [PubMed: 9496888]
47. Schettino G, Folkard M, Prise KM, Vojnovic B, Held KD, Michael BD. Low-dose studies of bystander cell killing with targeted soft X rays. Radiat Res 2003;160:505–511. [PubMed: 14565833]
48. Azzam EI, De Toledo SM, Spitz DR, Little JB. Oxidative metabolism modulates signal transduction and micronucleus formation in bystander cells from alpha-particle-irradiated normal human fibroblast cultures. Cancer Res 2002;62:5436–5442. [PubMed: 12359750]
49. Iyer R, Lehnert BE. Effects of ionizing radiation in targeted and nontargeted cells. Arch Biochem Biophys 2000;376:14–25. [PubMed: 10729186]
50. Azzam EI, de Toledo SM, Little JB. Stress signaling from irradiated to non-irradiated cells. Curr Canc Drug Targ 2004;4:53–64.
51. Morgan WF. Non-targeted and delayed effects of exposure to ionizing radiation: I. Radiation-induced genomic instability and bystander effects *in vitro*. Radiat Res 2003;159:567–580. [PubMed: 12710868]
52. Howell RW, Bishayee A. Bystander effects caused by nonuniform distributions of DNA-incorporated ^{125}I. Micron 2002;33:127–132. [PubMed: 11567881]
53. Persaud R, Zhou H, Baker SE, Hei TK, Hall EJ. Assessment of low linear energy transfer radiation-induced bystander mutagenesis in a three-dimensional culture model. Cancer Res 2005;65:9876–9882. [PubMed: 16267011]
54. Xue LY, Butler NJ, Makrigiorgos GM, Adelstein SJ, Kassis AI. Bystander effect produced by radiolabeled tumor cells in vivo. Proc Natl Acad Sci U S A 2002;99:13765–13770. [PubMed: 12368480]
55. Gerashchenko BI, Howell RW. Proliferative response of bystander cells adjacent to cells with incorporated radioactivity. Cytometry 2004;60A:155–164. [PubMed: 15290716]
56. Gerashchenko BI, Howell RW. Bystander cell proliferation is modulated by the number of adjacent cells that were exposed to ionizing radiation. Cytometry A 2005;66A:62–70. [PubMed: 15915508]
57. Gerashchenko BI, Howell RW. Cell proximity is a prerequisite for the proliferative response of bystander cells co-cultured with cells irradiated with gamma-rays. Cytometry 2003;56A:71–80. [PubMed: 14608634]

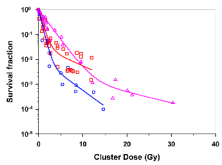

Figure 1.
Survival of V79 cells in multicellular clusters as a function of mean absorbed dose to the multicellular cluster. Data shown for experiments where 1% (△), 10% (□), or 100% (○) of cells in multicellular cluster were labeled with ^{210}Po-citrate. Curves represent least squares fits of the data to a biexponential function.

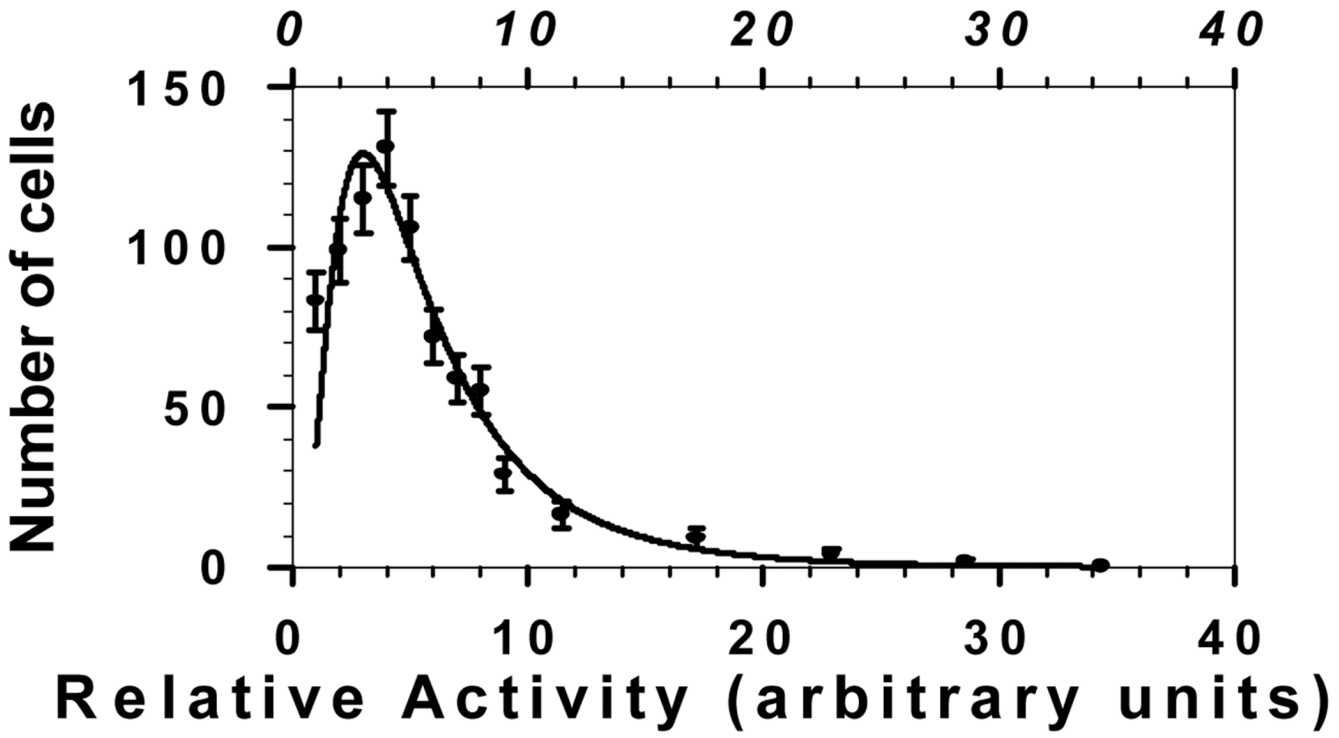

Figure 2.
Log normal distribution of intracellular ^{210}Po activity in V79 cells following a 30 min exposure of the population to a single extracellular concentration of ^{210}Po-citrate.